Astronomy & Astrophysics manuscript no. Mrk501˙tr February 23, 2006
(DOI: will be inserted by hand later)

Mrk 421, Mrk 501, and 1ES 1426+428 at 100 GeV with the CELESTE Cherenkov Telescope

D. A. Smith[1], E. Brion[1⋆], R. Britto[2], P. Bruel[3], D. Dumora[1], E. Durand[1], P. Eschstruth[4], P. Espigat[5], J. Holder[4], A. Jacholkowska[2], J. Lavalle[2], R. Le Gallou[1], B. Lott[1], H. Manseri[3], F. Münz[5], E. Nuss[2], F. Piron[2], T. Reposeur[1], and T. Sako[3]

[1] Centre d'études nucléaires de Bordeaux-Gradignan, Université Bordeaux 1, 33175 France (UMR 5797 CNRS/IN2P3)

[2] Laboratoire de physique théorique et astroparticules, Université Montpellier 2, 34095, France (UMR 5207 CNRS/IN2P3)

[3] Laboratoire Leprince-Ringuet, École Polytechnique, 91128 Palaiseau, France (UMR 7638 CNRS/IN2P3)

[4] Laboratoire de l'accélérateur linéaire, Université Paris 11, 91898 Orsay, France (UMR xxxx CNRS/IN2P3)

[5] Laboratoire d'astroparticule et cosmologie, Collège de France, 75231 Paris, France (UMR yyyy CNRS/IN2P3)

version: 23 February 2006

Abstract. We have measured the gamma-ray fluxes of the blazars Mrk 421 and Mrk 501 in the energy range between 50 and 300 GeV (1.4 to 4.8×10^{25} Hz). The signal from Mrk 421 is often strong. We compare its flux with previously published multi-wavelength studies and conclude that we are straddling the high energy peak of the spectral energy distribution. The signal from Mrk 501 in 2000 was weak ($3.4\,\sigma$). We have also found the flux from 1ES 1426+428 to be less than that half of the Crab near 100 GeV, which supports the view that the density of extragalactic starlight is lower than previously thought. The detector, called CELESTE, used up to 53 heliostats of the former solar facility "Thémis" in the French Pyrenees to collect Cherenkov light generated in atmospheric particle cascades. The data analysis and understanding of systematic biases have improved compared to previous work, increasing the detector's sensitivity.

Key words. BL Lacertae objects: individual: Mrk 421, Mrk 501, 1ES 1426+428 – Gamma-rays: observations

1. Introduction

Measurements of high energy emission from active galactic nuclei (AGN) give insights into a variety of open problems, such as the nature of the AGNs themselves, and the density and evolution of the extragalactic diffuse infrared background. After GLAST is launched in 2007 (Gehrels & Michelson 1999), the large number of high galactic latitude GeV gamma-ray sources to be seen will make AGNs become a background for searches for new classes of emitters – insufficient understanding of high energy AGNs might just limit potential glimpses of a hidden Universe.

Several AGNs of the "blazar" class emit above 250 GeV and have been detected by atmospheric Cherenkov imaging telescopes. Of these, Mrk 421 and Mrk 501 are the brightest (Błażejowski et al. 2005, Dwek & Krennerich 2005, Piron et al. 2001, Djannati-Ataï et al. 1997, Aharonian et al. 2003a). Until recently, the most distant blazar ($z = 0.129$) measured was 1ES 1426+428 (e.g. Djannati-Ataï et al. 2002, Petry et al. 2002). Using the similar distances of the two Markarians ($z \simeq 0.03$) and the relatively large distance to 1ES 1426+428, (Dwek & Krennerich 2005) were able to constrain the infrared background, via gamma-ray absorption by e^+e^- pair production off of diffuse infrared radiation. High infrared densities, and/or a *very* hard GeV/TeV spectrum for 1ES 1426+428, lead to predictions of Crab-like intensities for 1ES 1426+428 at 100 GeV. Recent results from HESS seem to exclude these high densities (Aharonian et al. 2005), nevertheless one of our early motivations was to use CELESTE to see whether in fact 1ES 1426+428 is gamma-bright. We conclude that it is not, which confirms the trend indicated by those two articles.

Another motivation was to test the Synchrotron Self Compton ("SSC") paradigm, consistent with most of the multiwavelength blazar data. For a detailed discussion of this class of models, with application to the blazars discussed in this paper, see for example (Tavecchio et al. 1998) or (Katarzyński et al. 2001). In its simplest variant, relativistic electrons generate synchrotron photons with a νF_ν peak in the optical to X-ray range, and then up-scatter these same photons to produce the peak seen in the GeV range. The inverse Compton peak position can be used to constrain the physical parameters of the model, and CELESTE was one of the first instruments sensitive near the Compton peak for these blazars. The peak lies beyond the energy range of the relatively large sample of EGRET blazars (Mukherjee et al. 1997). Mrk 501 in particular was visible to EGRET only during a flare (Kataoka et al. 1999).

Send offprint requests to: brion@cenbg.in2p3.fr

⋆ *C*urrent address: SAp, Commissariat à l'énergie atomique, 91191 Gif-sur-Yvette, France

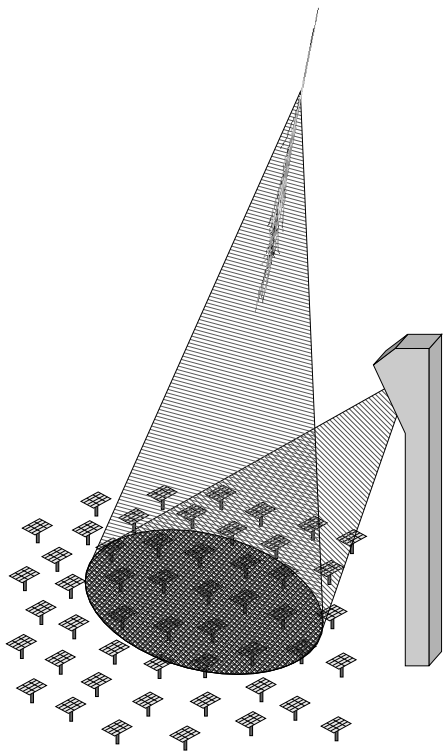

Fig. 1. Experimental principle: Heliostats tracking a source reflect Cherenkov light from atmospheric particle cascades to the secondary optics, photomultipliers, and acquisition electronics located high in the 100 meter tall tower.

CELESTE detected the Crab nebula in 1998 using a solar heliostat array (Smith 2000). STACEE, very similar to CELESTE, reported the flux above 190 GeV (Oser et al. 2001), followed by the flux above 60 GeV from CELESTE (de Naurois et al. 2002). STACEE recently measured the integral flux above 140 GeV from Mrk 421 (Boone et al. 2002) and, assuming power law spectral indices extrapolated from higher energies, bracketed the 50 to 700 GeV differential spectrum. A review of solar tower gamma-ray telescopes can be found in (Smith 2005).

This paper presents the first observations of three blazars below 100 GeV, by a solar heliostat array, and is structured as follows: we describe the detector, the analysis method, and the data samples. We emphasize improvements in our knowledge of the systematic uncertainties. We present light curves for the three blazars as well as the integrated fluxes, and place the results in the context of SSC models.

2. The CELESTE gamma-ray Telescope

The CELESTE detector is located in the eastern French Pyrenees (N. 42.50°, E. 1.97°, altitude 1650 m) and described in (Paré et al. 2002) and in (de Naurois et al. 2002). Figure 1 illustrates the principle. CELESTE was dismantled in June, 2004. Here we recall key features.

CELESTE used 53 heliostats (40 until 2001) of the Thémis former solar facility. The CAT Cherenkov imager ran on the same site (Piron et al. 2001 and references therein), as did the THÉMISTOCLE (Baillon et al. 1993) and ASGAT (Goret et al. 1993) Cherenkov sampling arrays. Each heliostat has a 54 m^2 mirror on an alt-azimuth mount. Light from the heliostats was reflected to a secondary optical system at the top of the 100 m tower, where one photomultiplier assembly (PMT) viewed each heliostat. Heliostat control and data acquisition systems were also high in the tower.

Data acquisition was triggered when the summed PMT pulseheight for at least N of the M groups of heliostats exceeded 4.5 photoelectrons ("p.e.") per heliostat. For the 40 heliostat array, $N = 3$ of $M = 5$ groups with 8 heliostats each was used most often. For the 53 heliostat array there were $M = 6$ trigger groups of between 6 and 8 heliostats each, and the trigger multiplicity was set at $N = 3, 4$, or 5 for different observations. The deadtime in the electronic delays depends on the rates, which depend on the threshold settings, which are determined in part by the choice of N. We took pains to remove these biases (Manseri 2004), in particular, with an offline group multiplicity cut based on the scaler rates. The acceptance shown in figure 5 has a offline multiplicity cut of 4 of 5, for illustration.

Each PMT signal was digitized at 1.06 nanoseconds per sample, with about 3 digital counts (dc) per photoelectron. 100 samples centered around the nominal Cherenkov pulse arrival time were recorded, providing event-by-event pedestal information that we used to determine the night sky background light for each channel. A second 28 sample window contained a timing reference pulse. Scaler rates, PMT anode currents, a GPS time stamp, and some meteorological information rounded out the data record.

3. Monte Carlo Simulations

CELESTE's first publication, on the flux from the Crab nebula quoted a $\sim$ 30 GeV threshold at the trigger level, and 60 GeV after analysis (de Naurois et al. 2002). We estimated the uncertainty on the energy scale to be less than 30 %, dominated by disagreement between predictions of Monte Carlo atmospheric cascade generators, and disagreement between estimated and observed PMT illuminations induced by bright stars. Monte Carlo studies have since shown that the CORSIKA Monte Carlo atmospheric shower generator best reproduces our experimental observables (Heck et al. 1998), and we use it for the results presented here.

Cherenkov photons from the shower generator are fed into a detailed simulation of our optics and electronics, to develop our data analysis methods and cuts, as well as to calculate the energy dependent effective area $A(E)$. Here we describe improvements made to the detector simulation since (de Naurois et al. 2002). The acceptances will be discussed after the analysis cuts have been explained.

3.1. Optical Throughput

Previously, the phototube illuminations when viewing stars were lower than predicted by the simulation. We reviewed the ray tracing programs, and found that two factors dominate the discrepancy. First, the combined heliostat and secondary mirror reflectivities are about 20 % worse than earlier measurements indicated [1]. Second, the simulated heliostat focussing was sharper than in reality. We compared the image sizes obtained from star "scans" used for heliostat alignment with simulated sizes, and modified the simulation to improve agreement. (In scans, we record PMT anode currents as the heliostats are pointed successively at a grid of points around the star position: see figure 7 in Paré et al. 2002).

Figure 2 illustrates a consequence of the ray tracing modifications. When tracking Mrk 421, the star 51 UMa (HD 95934, blue magnitude $M_{\rm B} = 6.16$) falls within the ± 5 mrad optical field-of-view for heliostats near the center of the array. The On-source PMT anode currents are thus larger ($i_{\rm On} \sim 13$ μA) than the Off-source currents which are due only to the diffuse night sky light ($i_{\rm Off} \sim 10$ μA). Using the PMT gains g, the current differences yield the star-induced illuminations $b = (i_{\rm On} - i_{\rm Off})/ge$, in photoelectrons per second (e is the electron charge). The figure shows that measured illuminations vary with the pointing direction, but less than was predicted by the original simulation. The simulations include the stars in the On and Off fields that contribute at least 5 % as much as 51 UMa, that is, $M_{\rm B} < 9.4$.

A few observations constrain the uncertainty in the optical throughput. Photometry using star scans yields 20 % channel-to-channel dispersion compared to the simulated values. A census of damaged heliostat mirrors, and the phototube manufacturer's measurements of the photocathode responses, combined together account for half of the dispersion. We attribute the rest to errors in the gains, and focussing anomalies for individual heliostats. However, what matters most is the sums over the 8 heliostats of the trigger groups: the *total* variation over the 5 groups is ± 15 %. We conclude that the overall effect on the gamma-ray energy scale of the uncertainty in the optical throughput is less than 10 %. Finally, we remark that the gamma-ray energy scale predicted by the Monte Carlo simulation shifts less than figure 2 suggests, since an atmospheric shower is a light source of angular extent comparable to the detector field-of-view, and so the effect of heliostat "defocussing" is less violent for showers than it is for the point-like stars.

Since the earlier work, the electronics simulation has been completely re-written, leading to improved agreement between predicted and observed signals, in the trigger, and for single channels. The good agreement for the final ξ analysis variable, described

[1] We thank Professor Ladislav Rob of Charles University, Prague, and his colleagues at Compas Ltd., Turnov, Czech Republic, for the recent measurements.

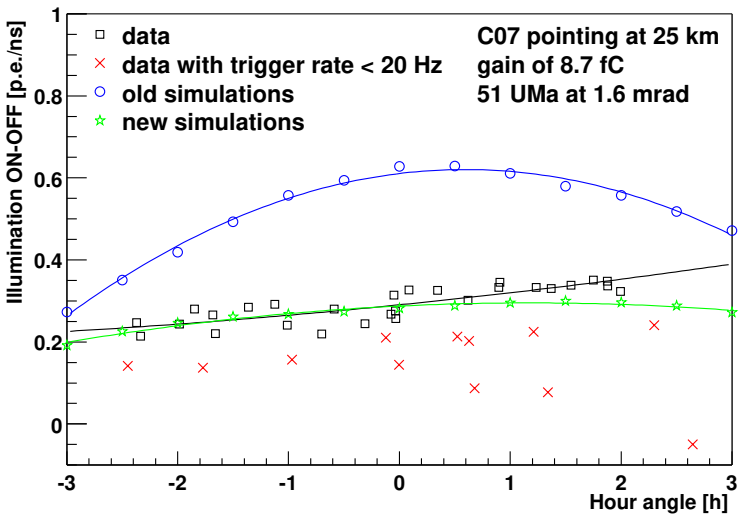

Fig. 2. Example of phototube illuminations induced by the star UMa 51 in the field of view of Mrk 421, versus hour angle, for heliostat C07. Squares & crosses: For the 40 pairs of On- and Off-source "double-pointing" data runs passing current and rate stability criteria, the quantity shown is the difference of the average current during each run divided by the PMT gain g, $(i_{\rm On} - i_{\rm Off})/ge$. For the crosses, the trigger rates were stable but lower than usual: optical transmission was low, presumably due to clouds or frost, and these runs were rejected. Circles: Original detector simulation. Stars: Simulation results, after "defocussing" the heliostats and degrading the mirror reflectivities as described in the text.

below, is the result of the care taken to model the elements of the complex electronics chain.

3.2. Atmospheric Transmission

The amount of Cherenkov light that reaches the ground varies between different sites and seasons depending mainly on the aerosol content versus altitude (Bernlöhr 2000). The same also holds for atmospheric extinction in stellar photometry (Hayes & Latham 1975). The effect on CELESTE is particularly striking: the $\sim$ 25 Hz cosmic ray trigger rates for winter sources (*e.g.* Crab and Mrk 421) decrease to under 15 Hz every year in spring, affecting sources like Mrk 501 and 1ES 1426+428. Table 1 lists the fraction of the data sets above and below 15 Hz.

The CORSIKA Monte Carlo provides a choice of tabulated wavelength and altitude dependent extinction curves. The default contains some aerosols. The Palomar curve from (Hayes & Latham 1975) used for our stellar photometry studies contains fewer aerosols, for an integrated transmission above Thémis at 400 nm 6 % greater than for the CORSIKA curve.

One of us used an amateur telescope with filters and a CCD camera to measure the total integrated atmospheric transmission during some nights when the trigger rates were

above 20 Hz. He used the apparent brightness of several stars as a function of their zenith angles (Boguer method), at three wavelengths (blue: 390-490 nm, green: 500-560 nm, and red: 610-660 nm). The Cherenkov light recorded by CELESTE is mainly in the blue range. The CCD results show that the sky at Thémis corresponds to the Palomar extinction curve. We made a CORSIKA extinction table corresponding to the Palomar curve which we use to simulate good running conditions.

To calculate the acceptances for data acquired with trigger rates < 15 Hz we made another CORSIKA extinction table that we call "dirty". We increased the aerosol contribution to the Palomar curve so that the integrated transmission above Thémis at 400 nm is 60 % less. This choice comes from two observations. The first appears in figure 2, where the phototube illumination due to the bright star near Mrk 421 in good conditions is halved for data acquired with a low trigger rate. The second is that we simulated proton showers using both extinction tables, and reproduced both the nominal and the degraded trigger rates.

Figure 5 shows the acceptance curves obtained for the two atmospheres, used to convert our gamma-ray rates to fluxes, as discussed below.

For the record, a custom-built LIDAR operated at Thémis along with CELESTE ultimately contributed little to our mastery of the atmosphere, due to difficulties with the quantitative interpretation of its data.

4. Data Samples

Maximum Cherenkov emission for 100 GeV γ-ray showers occurs around 11 km above the site. For CELESTE's oldest data, the heliostats were aimed at this height in the direction of the source, to maximize Cherenkov light collection. This is called Single Pointing data (SP).

SP provides the lowest energy threshold, but also decreases the detector's sensitive area. For one season we took data in a configuration called Double Pointing (DP), where half the heliostats point at 11 km and the rest at 25 km. This increases the area and improves cosmic ray rejection, while raising the energy threshold only slightly.

Our ± 5 mrad field-of-view matches the apparent size of a gamma shower, to optimize the ratio of Cherenkov light to night sky background light. Tails of cosmic ray showers are outside the field-of-view, reducing background at the trigger level but weakening offline rejection. In 2001 we added 13 heliostats to CELESTE, and thereafter pointed 41 heliostats at the 11 km point, and the remaining 12 at a ring 150 meters around the point. The 12 "veto" heliostats can see shower tails outside the central field-of-view, enhancing cosmic ray rejection (Manseri 2004). We call this Single Pointing with Veto data (SPV).

Source	SP	DP	SPV	All pairs	< 15 Hz	On hours
Mrk 421	61	44	28	133	20 %	38.9
Mrk 501	10	25	–	35	50 %	10.3
1ES 1426+428	–	–	33	33	40 %	8.8

Table 1. Number of data pairs, after applying stability criteria to the PMT anode currents and to the trigger rates. Single Pointing (SP), Doubling Pointing (DP), and Single Pointing with Veto (SPV) are explained in the text. The fraction of the data set with a cosmic ray trigger rate below 15 Hz, which we ascribe to seasonal increases in atmospheric extinction, is also listed.

Ultimately the performance of the ξ analysis was such that the veto rejection was not used. But the 12 veto heliostats around the edge of the heliostat field led us to restructure the trigger into $M = 6$ groups. The changed trigger topology affects the shape of the recorded showers, leading to different energy dependent acceptances.

Source observations ("On") last about 20 minutes and are followed or preceded by an observation at the same declination, offset by 20 minutes in right ascension. "Off" data gives a reference for the cosmic ray background – the signal is the difference between On and Off, after analysis cuts. However, changes in sky conditions between On and Off can cause differences having nothing to do with gamma-rays: we select stable On-Off pairs with a cut on the χ^2 value obtained from a least-squares fit to a constant PMT anode current versus time, and to the trigger rate versus time, for both runs. We also rejected pairs with very low data rates (< 10 Hz), or anomalously high trigger dead times. The weather at Thémis is fickle, and we rejected over half of our data.

Table 1 lists the data sets, recorded during clear, moonless nights from December 1999 through May 2004, after data selection.

5. Data Analysis

Since (de Naurois et al. 2002) we have changed our analysis strategy, as described below. The Flash ADC data quality improved, which helps wavefront reconstruction. Our procedures to remove the biases induced by night sky background differences at the trigger level ("software trigger") and in the FADC data ("padding") have been refined. Overall sensitivity compared to (de Naurois et al. 2002) has more than doubled.

Just above the trigger threshold, the Cherenkov signal in one channel is comparable to the fluctuations of the night sky background light. Summing the channels greatly improves the signal-to-noise ratio, after correcting for the propagation delay to each heliostat, assuming a spherical Cherenkov wavefront. Lacking knowledge of the shower core position, we scan the plane at 11 km and evaluate the ratio H/W for each point in a grid, where H and W are the height and the width of the summed signal (see figure 3). The grid position giving the largest value of the ratio H/W is a measure of the shower

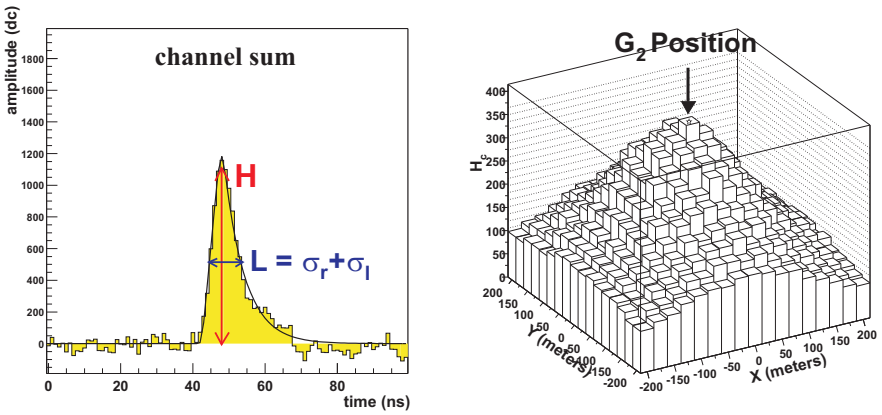

Fig. 3. LEFT: Summed Cherenkov pulse – a 100 ns Flash ADC window, centered at the time an ideal spherical wavefront 11 km directly above the site would reach the photomultiplier tubes after reflection from the heliostats, is recorded for each channel. In analysis, we repeatedly sum the 40 (SP and DP data) or 41 (SPV data) channels over a grid of hypothetical shower core positions, and keep the maximum value of the ratio $(H/W)_{\max}$ (sum height H over sum width W). RIGHT: The H/W values for each position of the grid, for a single simulated event. The grid position with $(H/W)_{\max}$ is a good ($\pm$15 m) estimator of where the gamma-ray would have hit the ground. The analysis variable $\xi = (H/W)_{\max}/(H/W)_{200\ \mathrm{m}}$ is normalized to the ratio $(H/W)_{200\ \mathrm{m}}$ averaged 200 meters from the grid center.

core position. The wavefront sphericity correlates with how much H/W decreases 200 m away from the shower core. This relative decrease, called ξ, is shown in figure 4 for an Off observation, Mrk 421 On-Off data, and for a simulation of a γ-ray spectrum. The Cherenkov wavefront from γ-ray induced showers is, on average, more spherical than for showers initiated by charged cosmic rays and, as expected, γ-ray showers have smaller ξ than hadronic showers. (Simulations indicate that the trigger rate is dominated by 18 Hz of protons, with 4 Hz of helium nuclei.)

The ξ distributions change for different heliostat pointings. This article concerns three blazars with similar declinations, all transiting near zenith at Thémis, so the only changes are the pointing configuration and the hour angle of the data. We studied simulations and the strong signals from Mrk 421 and the Crab to find the optimum ξ cuts: we chose the value $\xi < 0.4$ as a good compromise between a high efficiency for gamma-rays with a correspondingly small systematic uncertainty, versus the slightly statistical significance we obtain with tighter cuts adapted to the many different pointings, but for which our systematic uncertainties are larger.

To summarize CELESTE's performance: for one hour of On-source Crab data near transit, analysis using $\xi < 0.4$ gives a significance of 3.3 σ for SP and DP data, and 5 σ for SPV. Optimized cuts increase this by 20 % (and more for Mrk 421). We keep 9 ± 2 gamma/min after $\xi < 0.4$ cuts. The RMS of the normalized pair-by-pair residuals about the average rate is 1.2, where a value of 1 indicates that the

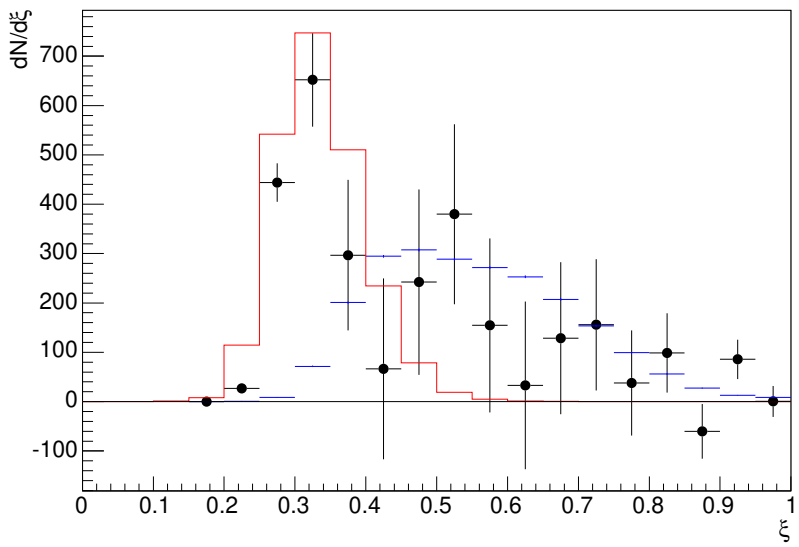

Fig. 4. ξ distributions for Mrk 421 for March 2004 data. Black dots show On-Off data. The broad histogram is Off data (*i.e.* cosmic ray background). The narrow histogram is simulated gamma-rays. The simulation and Off data are normalized to the number of On-Off events.

light curves are free of systematic biases. Folding our energy dependent acceptance $A(E)$ (similar to figure 5) with the Crab inverse Compton spectrum parametrized in table 6 of (Aharonian et al. 2004) yields a maximum at 90 GeV. The rate falls to 20 % of the maximum below 50 GeV and above 300 GeV. The flux thus obtained is $2.0 \pm 0.12 \times 10^{-11}$ erg cm^{-2} s^{-1}, in good agreement with expectations at this energy, and higher than our previous result in de Naurois et al. 2002, although within the uncertainties. The flux obtained for SP, DP, and SPV data is the same, within the statistical fluctuations.

6. Results and Discussion

Tables 2, 4, and 5 summarize the data analysis results for the three blazars Mrk 421, Mrk 501, and 1ES 1426+428, respectively. For a gamma-ray source with differential spectrum $\phi(E)$ the number N of detected gammas will be

$$N = T \int_0^\infty A(E)\phi(E)\mathrm{d}E$$

where T is the On-source time and $A(E)$ is the energy dependent gamma-ray collection area obtained from the Monte Carlo calculations. We have calculated $A(E)$ for each heliostat configuration, and for hour angles of $(0, 0.5, 1.0, 1.5, 2.0)$ hours, for each of the two atmospheres described above. Figure 5 shows $A(E)$ at the trigger level, and after cuts, for the direction of the blazar Mrk 421 ($\delta = 38°$), one hour after transit. (The few degree discrepancy with the other two blazar's declinations induces a negligible error). For the blazar spectra we assume a power law, $\phi(E) = kE^{-\alpha}$, for a constant k.

Figures 6, 7, and 8, show the acceptance-corrected light curves for the blazar Mrk 421 during the years 2000, 2001, and 2004 seasons. Figures 11, and 13 show the light curves for Mrk 501, and 1ES 1426+428. The curves assume power laws with spectral index $\alpha = 2$. There is an often strong signal from Mrk 421, and no signal for 1ES 1426+428. The excess in the Mrk 501 data is discussed below. For the fluxes shown on the SEDs (Spectral Energy Distributions) in figures 9 and 12) we vary between $\alpha = 1.8$ and $\alpha = 2.2$ to estimate the uncertainty due to the choice of α. (CELESTE's energy range is near the SED high energy peak for these three blazars, where $\alpha \equiv 2$.) CELESTE presented an energy reconstruction method in (Piron et al. 2003) which was used to search for a signal in energy bands in (Lavalle et al. 2005) but which is not applied here.

The systematic uncertainty on the CELESTE fluxes has different causes. As stated, since (de Naurois et al. 2002) we improved the Monte Carlo shower generation, and the detector simulation now reflects our enhanced knowledge of the optical throughput and of the electronics chain. We believe that the error on our absolute energy scale for data acquired in nominal conditions is less than 20 %. The largest remaining uncertainty comes from the varying atmospheric transmission. We make a first-order correction by grouping the data into subsets with trigger rates of ≤ 15 and > 15 Hz (see table 1) for use with the nominal or "dirty" acceptances, $A(E)$, as in figure 5. This correction is large: the effective area $\langle A \rangle = \dfrac{\int_0^\infty A(E)\phi(E)\mathrm{d}E}{\int_0^\infty \phi(E)\mathrm{d}E}$ is half as large with the "dirty" atmosphere. If the trigger rates were uniformly distributed between the observed extrema of 12 and 24 Hz, the dispersion introduced into the fluxes by grouping the data would be about 25 %. In fact, the trigger rates cluster around two values and this bias is thus smaller. The dependence of $\langle A \rangle$ on the spectral index α further biases the flux, by less than 20 % for $\alpha = 2 \pm 0.2$.

Data set	Cut	Number of events			Significance	Signal-to-noise	Excess
		N_{On}	N_{Off}	$N_{\mathrm{On}} - N_{\mathrm{Off}}$	N_σ	$\frac{N_{\mathrm{On}}-N_{\mathrm{Off}}}{N_{\mathrm{Off}}}$ [%]	[γ/min]
SP (17.8 h)	Raw Data	1 575 396	1 557 192	18 204	8.8	1.2	17.0
	Software trigger	1 056 705	1 044 811	11 893	7.1	1.1	11.1
	All cuts	276 057	270 113	5 945	7.1	2.2	5.6
DP (12.9 h)	Raw Data	983 550	961 257	22 293	14.3	2.3	28.7
	Software trigger	532 883	523 661	9 223	8.1	1.8	11.9
	All cuts	113 507	106 904	6 603	12.8	6.2	8.5
SPV (8.2 h)	Raw Data	621 243	604 926	16 317	13.0	2.7	33.3
	Software trigger	410 429	401 791	8 638	8.5	2.1	18.3
	All cuts	62 914	57 551	5 362	13.9	9.3	11.8
All data (38.9 h)	Raw data	3 180 189	3 123 375	56 814	19.7	1.8	24.3
	Software trigger	2 000 017	1 970 264	29 753	13.1	1.5	12.7
	All cuts	452 478	434 568	17 910	16.9	4.1	7.7

Table 2. Number of events before and after cuts, for the Mrk 421 data sets.

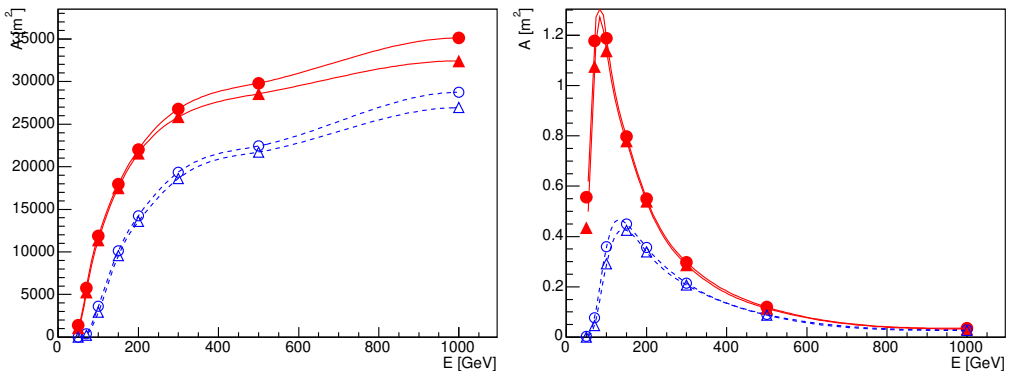

Fig. 5. Energy dependent gamma-ray collection area $A(E)$, at the trigger level (round markers), and after analysis cuts (triangles), for sources culminating near zenith, 1 hour after transit, for 11 km single pointing (SP). The curves are splines. The top two (solid) used the low-aerosol atmosphere while the bottom two (dashed) used the "dirty" atmosphere (see text). During analysis, a trigger group multiplicity cut of $N = 4$ of the $N = 5$ groups was applied.

Epoch	ASM (a)	PCA	CAT (d)	HEGRA (e)	VERITAS (f)	CELESTE (g)
2000 Feb 4	1.17 ± 0.08 (h)		189.7 ± 21.2	11.24 ± 3.41		2.05 ± 0.35
(51577.99 to 51578.18)						
2000 Feb 10	1.12 ± 0.12 (h)	1.41 ± 0.02 (b)	85.3 ± 19.7	2.43 ± 1.93		1.06 ± 0.31
(51583.99 to 51584.18)						
2000 Feb 27 to March 12	0.37 ± 0.07		48.3 ± 10.9	3.9 ± 0.8		0.61 ± 0.14
(51601.96 to 51615.09)						
2001 Feb (4 nights)	2.41 ± 0.34 (h)		208.7 ± 10.5	22.5 ± 0.8	1.05 ± 0.07	2.31 ± 0.21
(51956.98 to 51963.11)						
2001 April 14 to 17	1.27 ± 0.20		131.7 ± 16.3	18.7 ± 3.1	1.12 ± 0.05	0.96 ± 0.32
(52012.90 to 52015.97)						
2003 Feb to April	0.71 ± 0.03	17.3 ± 0.02 (c)			0.94 ± 0.04	1.45 ± 0.31
(52667.12 to 52762.94)						
2004 Feb 15 to 18	2.87 ± 0.26	39.3 ± 0.1 (c)			1.66 ± 0.20	2.13 ± 0.22
(53050.05 to 53053.08)						
2004 March 16 to 18	1.28 ± 0.50	48.4 ± 0.2 (c)			3.37 ± 0.17	1.43 ± 0.19
(53079.91 to 53082.02)						

Table 3. Multiwavelength fluxes from Mrk 421 coincident with CELESTE data. (a) ASM quick-look results provided by the ASM/RXTE team are in counts per second (http://xte.mit.edu/ASM_lc.html). RXTE PCA 2-10 keV fluxes are in (b) 10^{-10} erg cm^{-2} s^{-1}, 3-20 keV (Krawczynski et al. 2001), and in (c) counts per second (Błażejowski et al. 2005). (d) CAT fluxes are in 10^{-12} photons cm^{-2} s^{-1}, $E > 0.3$ TeV (Piron et al. 2001). (e) HEGRA fluxes are in 10^{-12} photons cm^{-2} s^{-1}, $E > 1$ TeV (Krawczynski et al. 2001, Aharonian et al. 2003a). (f) VERITAS fluxes above 300 GeV are in gamma/min, where the Crab gave 2.40 (2.93) gamma/min for 02/03 (03/04) (Holder et al. 2001, Błażejowski et al. 2005). (g) CELESTE fluxes are in 10^{-9} photons cm^{-2} s^{-1}, $E > 0.09$ TeV. (h) means of $\pm$ 2 nights.

6.1. Mrk 421

Understanding blazars requires observations at different wavelengths, preferably simultaneous given these object's variability. Happily, much of our data coincides with previously

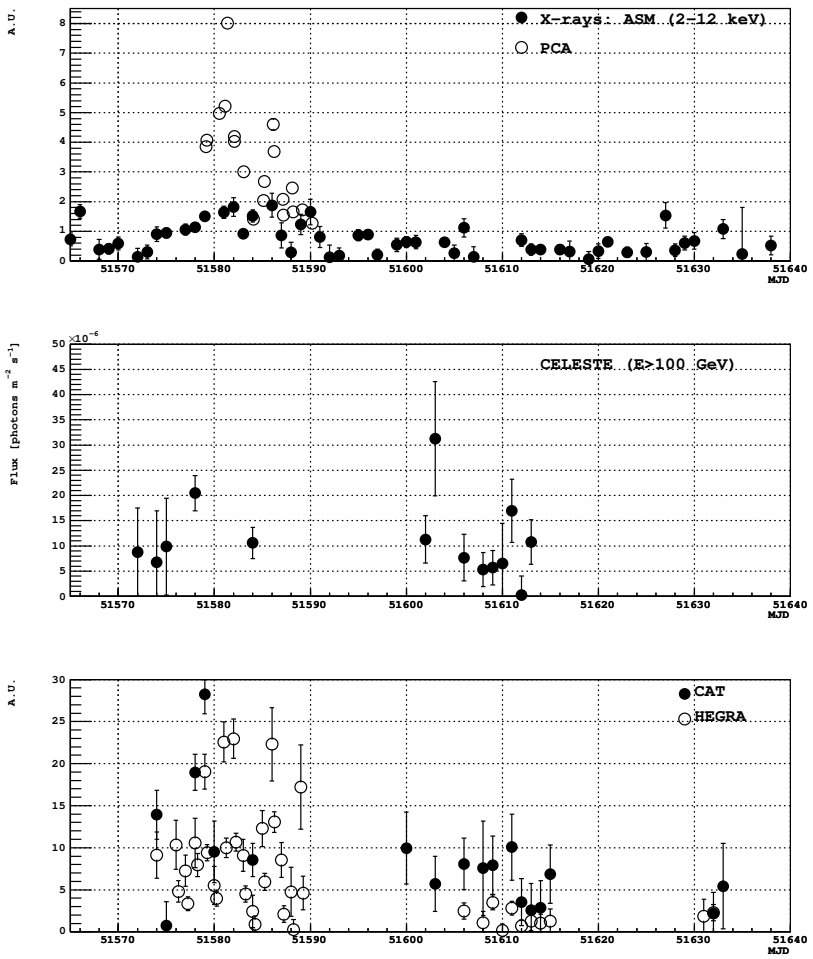

Fig. 6. Mrk 421 from February 27 to March 12, 2000. Big red dots are CELESTE daily averages (this work). Open triangles are from CAT (Piron et al. 2001). Blue dots are from Hegra – big dark ones from (Krawczynski et al. 2001) and lighter smaller ones from (Aharonian et al. 2002). Squares are RXTE ASM daily averages and crosses are RXTE PCA from (Krawczynski et al. 2001).

published results. Table 3 lists the CELESTE, TeV, and X-ray fluxes for the epochs with CELESTE data. Our Mrk 421 results suggest that the high energy peak of the SED lies in CELESTE's energy range.

The notion that blazar SEDs have a two-bump structure is widely accepted. But in fact, EGRET saw peaks, near 1 GeV, for very few blazars (Mukherjee et al. 1997), and the even smaller number of TeV blazar detections are beyond the peak, with the possible exception of Mrk 501 (a sample of spectra is shown in (Schroedter et al. 2005)). The two-peak picture is closely related to the SSC paradigm, that is, to particle acceleration in AGNs being mainly electronic. Yet, AGN are often cited as the accelerators of high energy cosmic rays in which case heavy ion acceleration must also occur, and it is therefore useful

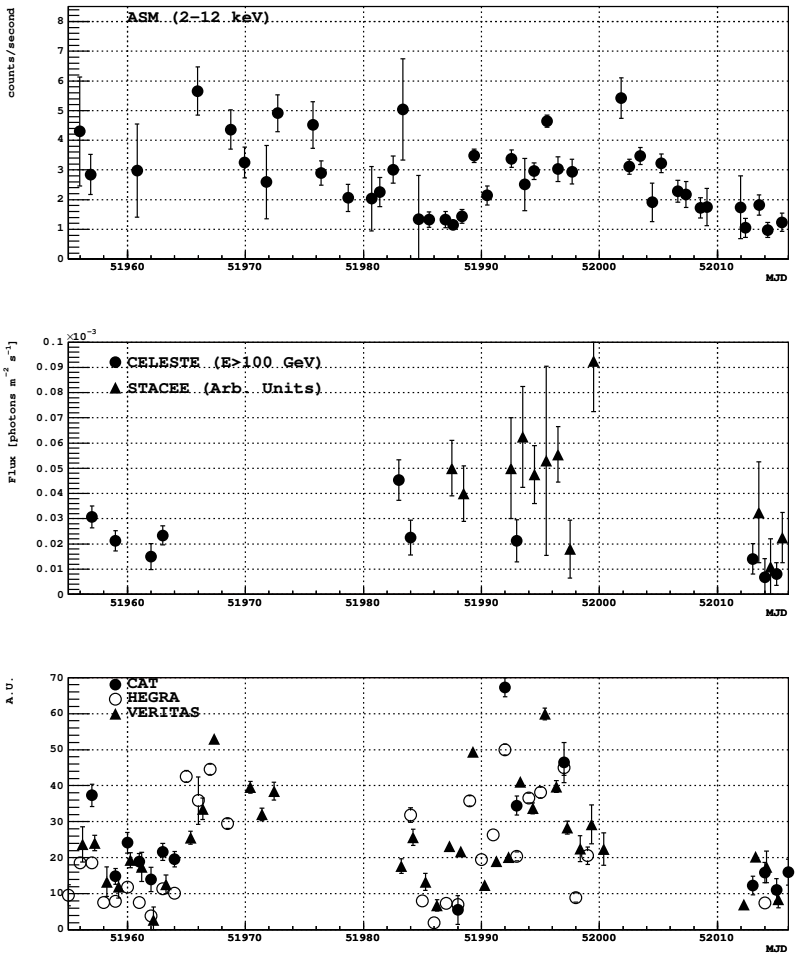

Fig. 7. Mrk 421 in 2001. Big red dots are CELESTE daily averages (this work). Open triangles are from CAT (Piron et al. 2001). Blue dots are from Hegra – big dark ones from (Krawczynski et al. 2001) and lighter smaller ones from (Aharonian et al. 2002). Squares are RXTE ASM daily averages and crosses are RXTE PCA from (Krawczynski et al. 2001).

to know whether the high energy peak really exists. We now argue that the CELESTE results are consistent with a peak near 100 GeV for Mrk 421.

To start, March 2000 was CELESTE's richest data taking period, with 11 of 14 consecutive nights (from 2000 February 27 to March 12, MJD 51601.96 to 51615.09). CAT (Piron et al. 2001) and HEGRA (Aharonian et al. 2002) have data for most of the same nights. Figure 6 shows the daily averaged data for this period. All four experiments with data at this epoch are at their lowest level in table 3. In February 2001, CELESTE recorded its highest flux levels, over 4 nights from MJD 51956.98 to 51963.11. Again, X-ray and TeV data agree qualitatively. Finally, the CELESTE flux averaged over the 2003 season, from February through April (MJD 52667.12 to 52762.94) was at an intermediate level, roughly tracking the other experiments.

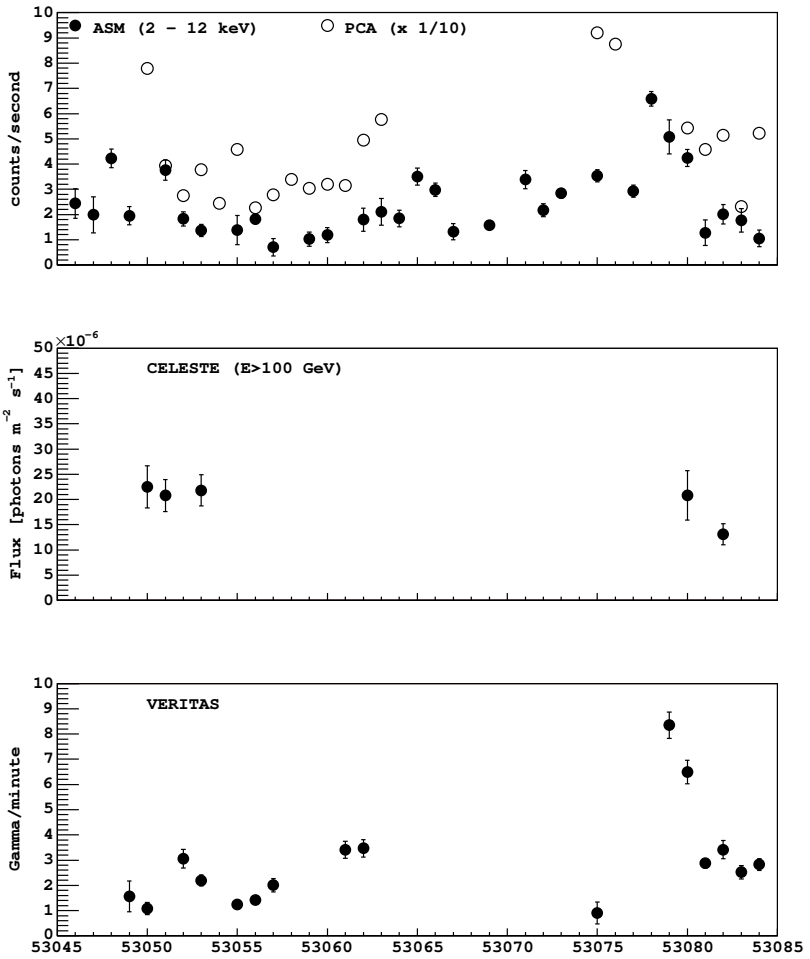

Fig. 8. Mrk 421 in February and March 2004.

More quantitatively, figure 9 shows the SED for Mrk 421 taken from (Błażejowski et al. 2005) to which we have added our result for an epoch when X-ray rates from the PCA on RXTE and TeV data from Cherenkov imagers are available. Specifically, CELESTE has seven data runs for each of the nights of 2000 February 4 (MJD 51577.99 to 51578.18) and 2000 February 10 (51583.99 to 51584.18), with signals of 13.6 ± 2.6 and 6.5 ± 2.0 gamma/min, respectively. CAT (Piron et al. 2001) and HEGRA (Krawczynski et al. 2001) report fluxes for both nights. The HEGRA paper includes 3-20 keV an X-ray flux measurement for February 10 from the PCA on RXTE of 1.4×10^{-10} ergs cm^{-2} s^{-1}, that is, on the "low" X-ray curve as defined in (Błażejowski et al. 2005). We normalized the CAT spectrum for 2000 to CAT's average flux for those two nights (reduction by a factor 0.7) and added it to the SED. We see that the CELESTE and CAT fluxes agree and correspond to the "low" model curve at high energy.

That our data agree with their model does not mean that peak really exists, so we turn to the light curves. The detailed multi-wavelength study reported in (Błażejowski et al. 2005) makes February-March 2004 particularly interesting.

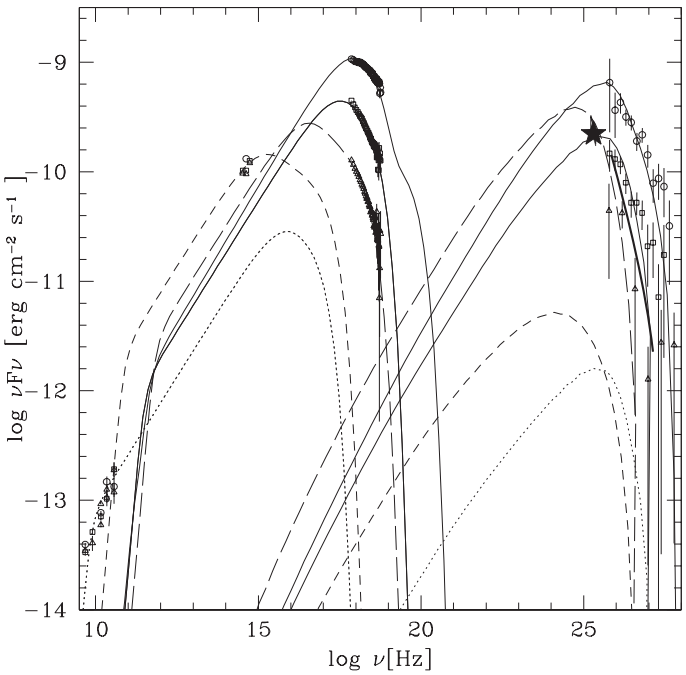

Fig. 9. CELESTE average flux measurement (black star) for Mrk 421 for 2000 February 4 (MJD 51578) and February 10 (51584), superimposed on the spectral energy distribution from the multiwavelength study by (Błażejowski et al. 2005). The X-ray activity level for February 10 from (Krawczynski et al. 2001) corresponds to the "low" activity state. The CAT spectrum for the year 2000 in (Piron et al. 2001) has been normalized for the flux measured by CAT for those nights (thick black line).

CELESTE measured a steady high state of 19 ± 3 gamma/min for the three nights of 2004 February 15 to 18 (MJD 53050.05 to 53053.08), brighter than the "medium state" discussed above, see table 3 and figure 8. VERITAS shows a steady low state, in seeming contrast to CELESTE. But figure 1 of (Błażejowski et al. 2005) shows an increasing optical flux on those dates, while PCA and ASM on RXTE show a decreasing X-ray state. This could be a shift of the low energy peak of the SED to lower energy. (Figure 1 of (Błażejowski et al. 2005) also shows that the radio flux is falling slowly, consistent with the end of a flare as seen far from the low-energy peak. In figure 9 the dotted line through the radio data comes from assuming a different acceleration zone than for the medium state X-ray and GeV-TeV curve, as is the dashed line through the optical data.) If the high energy SED peak also shifts during this epoch it could explain that CELESTE sees a high rate when VERITAS doesn't: VERITAS is above the SED peak while the CELESTE range straddles it.

Similarly, and also in figure 8, PCA and ASM show a declining X-ray state followed by a small rebound for 2004 March 16 to 18. For two nights of data (MJD 53079.91 to 53082.02) CELESTE has an average state of 9.2 ± 1.2 gamma/min, but here VERITAS sees the decline of the flare before returning to the low state. CELESTE's stability during VERITAS' changes is again consistent with 9, that is, with an SED peak at 100 GeV.

Recent spectral work on Mrk 421 by STACEE also seems to indicate that our 50 to 300 GeV energy range matches a high energy SED peak (Carson 2005). GLAST and VERITAS will map the high energy SED peaks in detail beginning in 2008 and will provide better insight.

Data set	Cut	Number of events			Significance	Excess
		N_{On}	N_{Off}	$N_{\mathrm{On}} - N_{\mathrm{Off}}$	N_σ	(min^{-1})
Year 2000 (8.3 h)	Raw data	616 194	613 337	2 856	2.1	5.8
	Software trigger	362 863	359 914	2 949	2.9	5.9
	All cuts	73 034	71 518	1 516	3.4	3.1
Year 2001 (2.0 h)	Raw data	130 820	131 584	−763	−1.3	-6.4
	Software trigger	67 040	67 410	−369	−0.9	-3.1
	All cuts	13 957	14 059	−102	−0.6	-0.85
All data (10.3 h)	Raw data	747 014	744 921	2 093	1.4	3.4
	Software trigger	429 903	427 323	2 580	2.4	4.2
	All cuts	86 991	85 578	1 414	2.9	2.3

Table 4. Number of events before and after cuts for the Mrk 501 data sets.

6.2. Mrk 501

The statistical significance of the excess for all the Mrk 501 data is weak (2.9 σ), as shown in table 4. The light curve in figure 11 shows that the excess comes mostly from the year 2000, with 3.4 σ for those four months. Figure 10 shows that the excess in 2000 ressembles a gamma-ray signal. However, changing the ξ cut values to those that optimize the statistical significance of the Mrk 421 signal do not enhance this excess, suggesting that taking the excess to be a gamma-ray signal is delicate.

CELESTE and the BeppoSAX X-ray satellite have data in common for four nights, from 2000 March 5 to 12, when Beppo measured between (0.76 ± 0.08) and $(1.18 \pm 0.12) \times 10^{-10}$ erg cm^{-2} s^{-1} (Massaro et al. 2004). The rates from ASM at these times are 0.41 ± 0.09 and 0.44 ± 0.09 cts/s, respectively. (ASM rates are unreliable at such low fluxes, nevertheless figure 11 shows that they track the Beppo measurements.) Averaging the ASM count rates for the nights with CELESTE data gives 0.44 ± 0.06 and 0.37 ± 0.09 for 2000 and 2001, respectively. The dispersion of the points is 0.5 cts/s for both seasons. Averaging ASM over longer periods gives essentially the same result, so that no significant difference in X-ray activity for the two years is apparent.

We believe that our experiment was stable and we choose to interpret the excess as due to gamma-rays from this well-known emitter. We use the same acceptances as for Mrk 421, again matched to the conditions of each data run. The flux at 110 GeV thus obtained for the year 2000 is $(1.24 \pm 0.42) \times 10^{-10}$ erg cm^{-2} s^{-1}. Combining both years changes

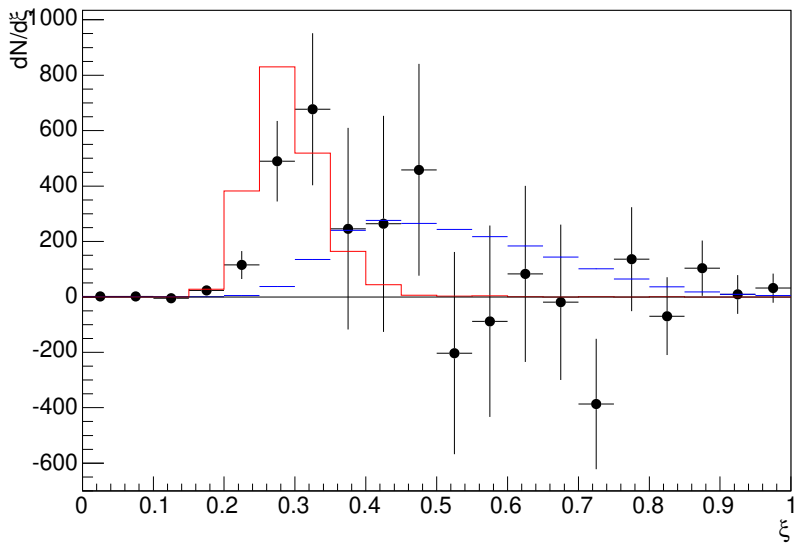

Fig. 10. ξ distributions for Mrk 501 for the year 2000 data. Black dots show On-Off data. The broad histogram is Off data (*i.e.* cosmic ray background). The narrow histogram is simulated gamma-rays. The simulation and Off data sets are normalized to the number of On-Off events.

the result to $(0.78 \pm 0.35) \times 10^{-10}$ erg cm^{-2} s^{-1}. The errors stated are statistical only. Figure 12 shows the flux superimposed on an SED taken from (Kataoka et al. 1999), with simultaneous ASCA x-ray and EGRET gamma ray data. We have added the BeppoSAX X-ray data taken at the same time as ours. Our flux measurement lies somewhat above the model expectations.

6.3. 1ES 1426+428

Table 5 and the light curve in figure 13 show that CELESTE detected no gamma-rays from the 1ES 1426+428, indicating that the flux at 80 GeV is less than 0.4×10^{-10} erg cm^{-2} s^{-1} (less than half the intensity of the Crab nebula). 1ES 1426+428 is one of the more distant blazars detected at TeV energies and has been used to constrain the density of extragalactic diffuse infrared light, possible because TeV photons can be absorbed by low energy photons via electron-positron pair production, $\gamma\gamma \rightarrow e^+e^-$. In particular, (Dwek & Krennerich 2005) took the spectra observed at high energies and, for a range of plausible assumptions about spectral shapes and infrared densities, established what the blazar's flux might be at CELESTE energies. For high densities the flux could be more intense than the Crab's. CELESTE's non-detection disfavors these high densities. In the same vein, the HESS array of imaging Tcherenkov detectors recently detected two distant blazars at TeV energies (Aharonian et al. 2005) and concluded that infrared densities are lower than was previously believed. CELESTE's non-detection supports this view.

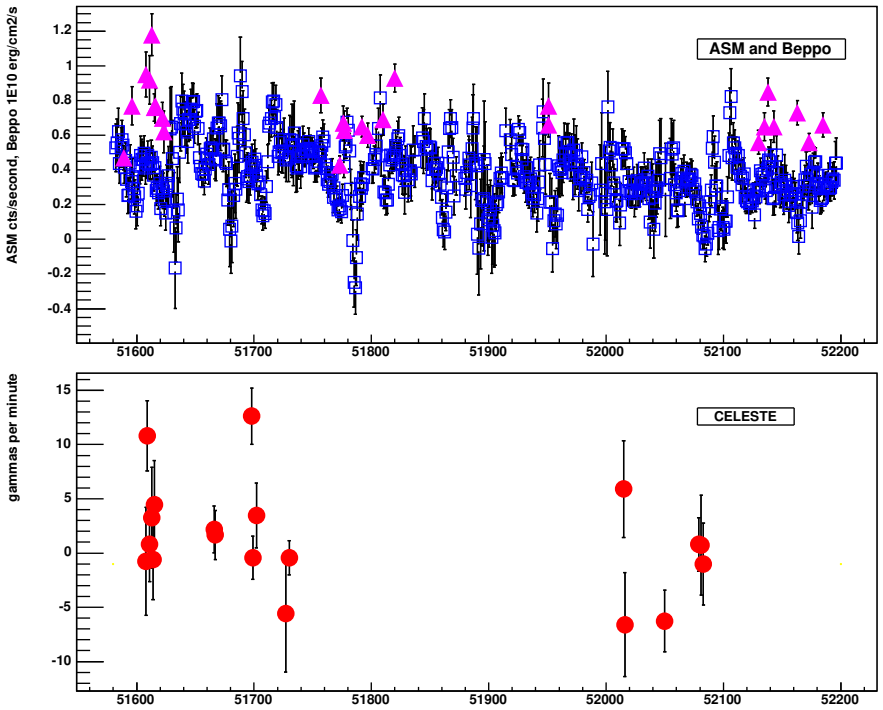

Fig. 11. Gamma- and X-ray light curves for Mrk 501. MJD 51600 and 52000 correspond to 26/02/2000 and 01/04/2001. TOP: 5-day running average of ASM 2 to 12 keV X-ray flux, in cts/s (squares), and BeppoSax 2 to 12 keV fluxes in 10^{-10} erg cm^{-2} s^{-1} (triangles), from (Massaro et al. 2004). BOTTOM: CELESTE nightly averages of the On-Off excess, in events per minute. Statistical errors only. May 2 (51666) is in this plot but needs to be thrown away for the final, acceptance-corrected version with fluxes instead of gammas per minute.

Data set	Cut	Number of events			Significance
		N_{On}	N_{Off}	$N_{On} - N_{Off}$	N_σ
All data (SPV, 8.8 h)	Raw data	675 340	673 239	2 101	1.6
	Software trigger	377 549	375 497	2 051	2.1
	All cuts	64 230	64 433	−204	−0.5

Table 5. Number of events before and after cuts for the 1ES 1426+428 data sets.

7. Conclusions

We have provided some of the first astrophysical flux measurements around 100 GeV, beyond the reach of EGRET on the Compton CGRO and below the range of previous ground-based telescopes, by recording atmospheric Cherenkov light with the reconverted solar tower power facility at Thémis. Our results for the blazar Mrk 421 help constrain the shape of the high energy peak of the spectral energy distribution. We have made the first detection of Mrk 501 in this range, although the detection is weak and the uncertainties on the flux are large. Finally, our non-detection of the distant blazar 1ES 1426+428 contribute to the growing evidence that the density of extragalactic infrared starlight

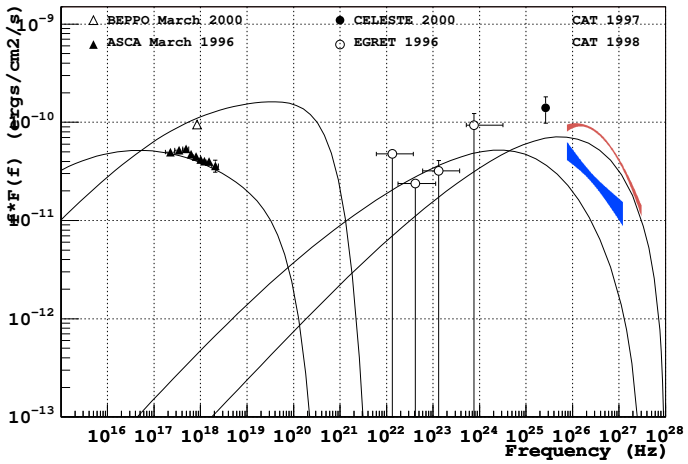

Fig. 12. CELESTE flux measurement for Mrk501 from the year 2000 (solid dot). The Beppo X-ray data (open triangle) is nearly simultaneous (Massaro et al. 2004). The EGRET data (open dots) and the ASCA X-ray measurements (solid triangles) are contemporaneous, and correspond to the SSC model curves (Kataoka et al. 1999). The X-ray state during CELESTE's detection was somewhat higher than for the EGRET detection. The TeV spectra are from the CAT Cherenkov imager: the lower is for the year 1998 (Khelifi et al. 2001), the higher is for the medium flare of 7 April 1997 (Djannati-Ataï et al. 1997).

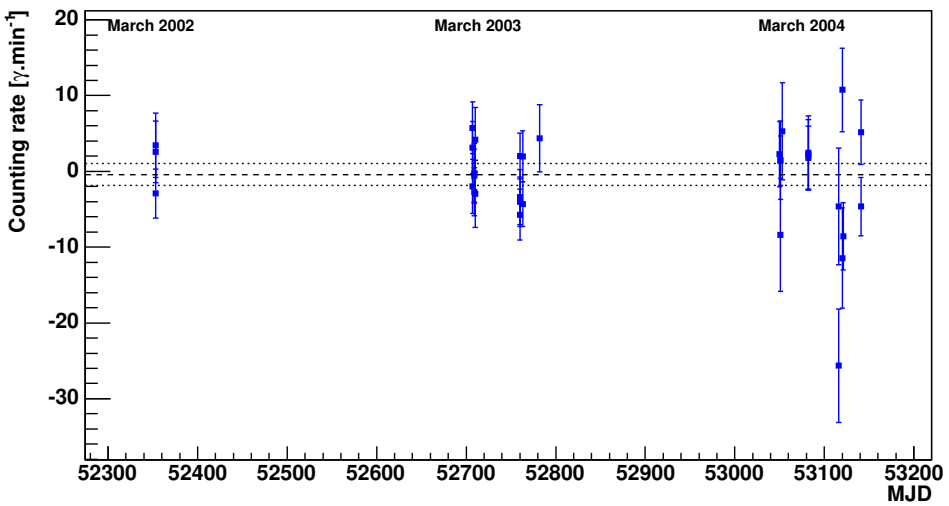

Fig. 13. Light curve for 1ES 1426+428 – no signal has been detected.

is lower than had been previously thought. Knowledge of this density is useful for the understanding of the evolution of galaxies in the Universe.

We have increased our detector sensitivity as compared to our earlier work, to a level near that predicted in our original proposal. The gain came mainly from a better analysis procedure but also from refinements in our detector simulation and electronics improvements. 80 % of the gamma-rays we detect have energies between 50 and 300 GeV. Bad

weather at our site lead to a low duty-cycle, resulting in a modest number of detections in spite of our dectector's good performance.

Acknowledgements. This work was supported by the IN2P3 of the French National Center for Scientific Research (CNRS) and by the Région Languedoc-Roussillon. We are grateful for the cooperation of Electricité de France. We thank Wei Cui, Jun Kataoka, and Dieter Horns for providing us with data files and macros.

References

Aharonian, F.A. et al., A&A 393, 89-90 (2002)

Aharonian, F.A. et al., A&A 410, 813-821 (2003)

Aharonian, F.A. et al., A&A 406, L9-L13 (2003)

Aharonian, F.A. et al., Nat. (2005), astro-ph/0508073

Aharonian, F.A. et al., ApJ 614, 897-913 (2004)

Baillon, P. et al., Astropart. Phys. 1, 341-355 (1993)

Bernlöhr, K., Astropart. Phys. 12, 255-268 (2000)

Błażejowski, M. et al., ApJ 630, 130-141 (2005)

Bruel, P., in proc. "Physics & Astrophysics in Space", Frascati (2004)

Boone et al., ApJL 579, 5-8 (2002)

Carson, J., doctoral thesis (2005), http://www.astro.ucla.edu/~carson/thesis/thesis.ps, ApJ in preparation

Cui, W., ApJ 605, 662-669 (2004)

Djannati-Ataï, A. et al., A&A 350, 17-23 (1997)

Djannati-Ataï, A. et al., A&A 391, L25-L28 (2002)

Dwek, E. & Krennerich, F., ApJ 618, 657-674 (2005)

Gehrels, N. and Michelson, P., Astropart. Phys. 11, 277-282 (1999)

Giebels, B. et al., Nucl. Instr. Meth. A 412, 329-341 (1998)

Goret, P. et al., A&A 270, 401-406 (1993)

Hartman, R.C. et al., ApJS 123, 79-202 (1999)

Hayes, D. S. and Latham, D. W., ApJ 197, 593-601 (1975)

Heck, D. et al., Report FZKAS 6019, Forschungszentrum Karlsruhe (1998)

Holder, J. et al., 27th ICRC, Copernicus Gesellschaft, Hamburg (2001)

Kataoka, J. et al., ApJ 514, 138-147 (1999)

Katarzyński, K., Sol, H. and Kus, A., A&A 367, 809-825 (2001)

Khelifi, B. et al. 27th ICRC, Copernicus Gesellschaft, Hamburg (2001)

Krawczynski et al., ApJ 559, 187-195 (2001)

Lavalle, J., Manseri, H., et al., A&A accepted (2005), astro-ph/0601298

Manseri, H., doctoral thesis (2004), http://doc.in2p3.fr/themis/CELESTE/PUB/papers.html

Massaro, E. et al., A&A 422, 103-111 (2004)

Mukherjee, R. et al., ApJ 490, 116 (1997)

de Naurois, M., Holder, J. et al., ApJ 566, 343-357 (2002)

Oser, S. et al., ApJ 547, 949-958 (2001)

Petry, D. et al., ApJ 580, 104-109 (2002)

Piron, F. et al., A&A 374, 895-906 (2001)

Piron, F. et al., 28th ICRC, Universal Academy Press, Tsukuba (2003)

Paré, E. et al., Nucl. Instr. Meth. A 490, 71-89 (2002)

Schroedter, M. et al., ApJ 628, 617-628 (2005)

Smith, D. A., Nucl. Phys. 80B, 163-172 (2000)

Smith, D. A., CELESTE internal note #53 (2004)

Smith, D. A., in proc. "Towards a Network of Atmospheric Cherenkov Detectors VII", Palaiseau (2005)

Tavecchio, F., Maraschi, L. and Ghisellini, G., ApJ 509, 608-619 (1998)

List of Objects

'Mrk 421' on page 1

'Mrk 501' on page 1

'Mrk 421' on page 3